Rare Metal Materials and Engineering
Volume 52, Issue 3, March 2023
Available online at www.rmme.ac.cn

Science Press

Cite this article as: Wang Hao, Yang Kun, Wang Jianzhong, et al. Preparation and Properties of Microporous Nickel with High Porosity[J]. Rare Metal Materials and Engineering, 2023, 52(03): 876-882.

ARTICLE

Preparation and Properties of Microporous Nickel with High Porosity

Wang Hao[1], Yang Kun[1], Wang Jianzhong[1], Shi Ying[1], Feng Peizhong[2], Huang Yuanping[1], Jing Peng[1], Akhtar Farid[3]

[1] State Key Laboratory of Porous Metal Materials, Northwest Institute for Nonferrous Metal Research, Xi'an 710016, China; [2] School of Materials Science and Physics, University of Mining and Technology, Xuzhou 221116, China; [3] Division of Materials Science, Luleå University of Technology, Luleå 97187, Sweden

Abstract: The strategy of sintered closed-hole followed by reopening was proposed to prepare the microporous nickel material with high porosity through the powder metallurgy and subsequential treatments. The carbonyl nickel powder with particle size of 1 μm was used as raw material, and the effects of sintering process parameters on the pore properties and mechanical properties of microporous nickel were studied. Results show that the porosity measured by mercury injection method of microporous nickel is 53.7%, and the average pore diameter is 612.25 nm at the sintering temperature of 400 °C. After machining, the porosity measured by mercury injection method is 54.0%, and the average pore diameter is 511.37 nm, which still satisfies the requirements of engineering application. The strategy provides providing a new approach for the preparation of microporous nickel and other porous metal materials.

Key words: high porosity; microporous structure; microporous nickel; preparation process; machining performance

Microporous materials with high porosity of >50% and pore diameter of <2 μm have many application potentials in the fields of fuel cells, noise reduction, heat insulation, and heat exchange. As a transition metal, nickel has excellent catalytic performance, good corrosion resistance, and fine machinability. Microporous nickel with high porosity has the excellent characteristics of both porous materials and metal nickel, thereby showing great potential in industry[1–3]. For the catalyst industry, nickel as a transition metal has excellent catalytic activity, and the micropores provide a larger specific surface area and abundant active sites[4–8]. As for filtration and separation, the microporous nickel has not only good corrosion resistance but also high efficiency of accurate filtration[9–10].

In the field of heat exchange, the characteristic of high porosity coupled with micro-size can improve the heat transfer efficiency. Higher porosity provides a channel for energy transmission, and the micropore structure can produce large driving force of liquid working medium flow. Meanwhile, the microporous nickel has good corrosion and heat resistance, which can ensure the long service life under different working fluids[11–15]. Wang et al[16] prepared the microporous nickel by traditional powder sintering method at the sintering temperature of 750–800 °C, which had porosity of 55%–64% and average pore diameter of 1.15–1.7 μm. Li et al[17] prepared microporous nickel with higher porosity at the sintering temperature of 700–900 °C by adding polymethyl methacrylate as the pore forming agent. The optimal average pore size is 2.37 μm and the porosity is 71.9%. In addition to organic pore forming agents, Li et al[18] prepared microporous nickel by adding soluble pore forming agents of NaCl and NiC_2O_4. Although the effect of powder metallurgy process and additives on microporous nickel has been widely discussed, few reports discuss the processability of microporous nickel. Due to the high heat exchange efficiency under harsh conditions and the miniaturization of lightweight components, the heat flux density in system is increased rapidly[19]. Therefore, the novel heat exchange elements, such as loop heat pipe (LHP), are required to effectively improve the heat exchange efficiency[20–22]. Currently, the conventional method of LHP evaporator is to prepare porous wick by powder metallurgy method. Then, the wick was assembled with dense

Received date: June 08, 2022
Foundation item: Science and Technology Department of Shaanxi Province (2021KJXX-75); National Natural Science Foundation of China (52020105011)
Corresponding author: Yang Kun, Ph. D., Professor, State Key Laboratory of Porous Metal Materials, Northwest Institute for Nonferrous Metal Research, Xi'an 710016, P. R. China, Tel: 0086-29-86231095, E-mail: yangk029@163.com

shell to form the evaporator and weld with other pipelines. The evaporator was processed into long slim pipe to improve heat exchange efficiency[23]. It is difficult to achieve the assembly accuracy only by near-net forming. If the gap between the dense shell and the porous wick is too large, the thermal resistance will seriously affect the heat exchange efficiency of the LHP system. Li et al[24] discussed two processing methods of nickel wicks in flat-plate LHP. After processing, the pore surface is blocked completely; while after wire-electrical discharge machining, the pore surface is treated by acid solution. Both processing methods have a strong influence on the pores, which are not conducive to the application of porous wick. For the engineering applications, the high-precision components of microporous nickel after processing require high assembly accuracy, effective heat exchange system, and original pore structures. Therefore, the processing performance of microporous nickel is crucial. In the machining process, the pores are easily deformed and blocked, thus reducing or losing their functions. Currently, the effect of machining parameters on the structure of microporous nickel is rarely reported.

In this research, the microporous nickel with satisfying porosity and pore size was prepared under cold isostatic pressing and low sintering temperature without adding pore forming agent and other sintering additives. The strategy of sintered closed-hole followed by reopening was proposed. The original porosity of microporous nickel was retained. This research provided a simple efficient method to prepare microporous nickel with high porosity and other metal porous materials.

1 Experiment

Carbonyl nickel powder with catenary morphology was used as raw material. The powder morphology observed by scanning electron microscope (SEM) is shown in Fig. 1. The characteristics and chemical composition of carbonyl nickel powder are shown in Table 1 and Table 2, respectively.

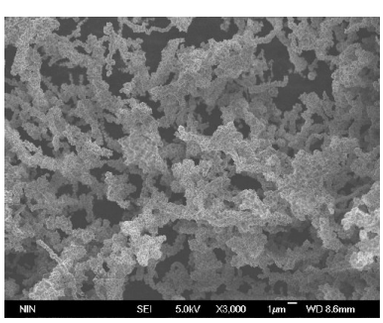

Fig.1 SEM morphology of nickel powder

Table 1 Characteristics of carbonyl nickel powder

Fisher particle size/μm	Apparent density/ g·cm^{-3}	Tap density/g·cm^{-3}
1.02	0.58	2.60

Table 2 Chemical composition of carbonyl nickel powder (wt%)

Fe	Co	C	O	S	Ni
<0.001	<0.001	<0.15	<0.15	<0.0015	Bal.

The carbonyl nickel powder was put into the package to determine its mass based on the package size. The cold isostatic pressing-sintering process was conducted by LDJ320/1500-300YS equipment. The pressing pressure was 10, 50, and 100 MPa, and the pressure holding time was 30 s. Then, the sintering was conducted in the sintering furnace (HL230) with the high purity hydrogen (purity of 99.99%) at ambient pressure and sintering temperature of 300–650 °C (±10 °C) for 1 h. The heating rate was 10 °C/min.

Porous nickel obtained at different sintering temperatures[13] was characterized and tested. The specimen shrinkage after compression and sintering was calculated. The morphology of raw powder and microporous nickel were observed by SEM (JSM-6460). Universal testing machine (ETM105D) was used to test the compression performance of microporous nickel. The maximum pore diameter was characterized by pore diameter detector (FBP-IV). The pore size distribution of porous nickel was characterized by the mercury injection method through mercury porosimeter (Autopore 9520). The subsequent machining performance was also analyzed by the digital controlled lathe (SK50P-01).

2 Results and Discussion

2.1 Effect of compressive pressure

The microporous nickel specimens after compression at 0, 10, 50, and 100 MPa followed by sintering at low temperature of 400 °C were analyzed. The changes of porosity and shrinkage of specimens under different compressive pressures are compared, as shown in Fig.2. Fig.3 shows the appearances of pressed microporous nickel specimens before and after sintering.

With increasing the compressive pressure from 0 MPa to 100 MPa, the shrinkage of microporous nickel before sintering is gradually increased to 26.4%. The increasing pressure aggravates the deformation of powder particles, which leads to the increase in shrinkage. For the microporous nickel specimens after compression and sintering, the internal

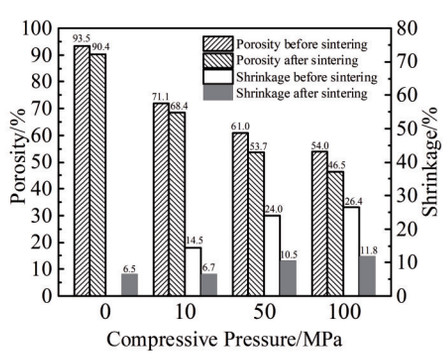

Fig.2 Porosity and shrinkage of different pressed microporous nickel specimens before and after sintering

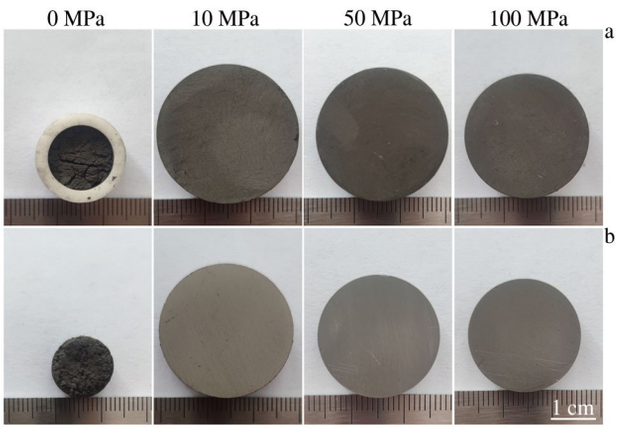

Fig.3 Appearances of different pressed microporous nickel specimens before (a) and after (b) sintering

stress in the powder particles is released in the sintering process, which increases the shrinkage. However, the increment is little: the shrinkage is increased from 6.5% to 11.8% with increasing the compressive pressure from 0 MPa to 100 MPa. In addition, with increasing the compressive pressure from 0 MPa to 100 MPa, the porosity of pressed microporous nickel specimens before sintering is reduced from 93.5% to 54.0%. This is because the bonding between particles is enhanced during compression, thereby forming the metallurgical bonding and resulting in the further reduction in porosity. After sintering, the porosity of pressed microporous nickel specimens is reduced from 90.4% to 46.5%. The porosity of less than 50% is unqualified. Thus, the optimal compressive pressure is 50 MPa, and the resultant porosity is 53.7%, which is still at the high porosity level. When the compressive pressure is lower than 50 MPa, the porosity cannot be easily controlled and the powder particles are not closely combined, resulting in the easy fall-off of powder particles and difficult shape control of specimens. Therefore, the compressive pressure of 50 MPa is selected as the fixed condition for further analysis of the effect of sintering process.

2.2 Effect of sintering temperature

Fig. 4 shows the effect of sintering temperature on the shrinkage and porosity of microporous nickel specimens. It can be seen that with increasing the sintering temperature, the changes in shrinkage and porosity of microporous nickel specimens show opposite variation trends. The shrinkage rate conforms to that based on sintering experience. With increasing the sintering temperature from 300 °C to 600 °C, the shrinkage is increased gradually from 2.0% to 25.4%; with further increasing the sintering temperature from 600 °C to 650 °C, the shrinkage is slightly reduced to 24.0%, indicating the dense material. The porosity of the specimens sintered at 600 and 650 °C is only 7.2% and 5.2%, respectively, indicating that the specimens are dense. Further densification requires even higher compressive pressure or longer holding time.

Fig.5 shows SEM morphologies of pressed specimens after sintering at different temperatures. When the sintering temperature is above 550 °C, the porosity and pore size of the specimens are reduced. According to the sintering experience,

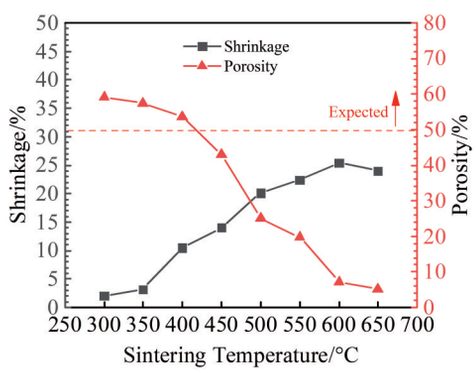

Fig.4 Effect of sintering temperature on shrinkage and porosity of microporous nickel specimens

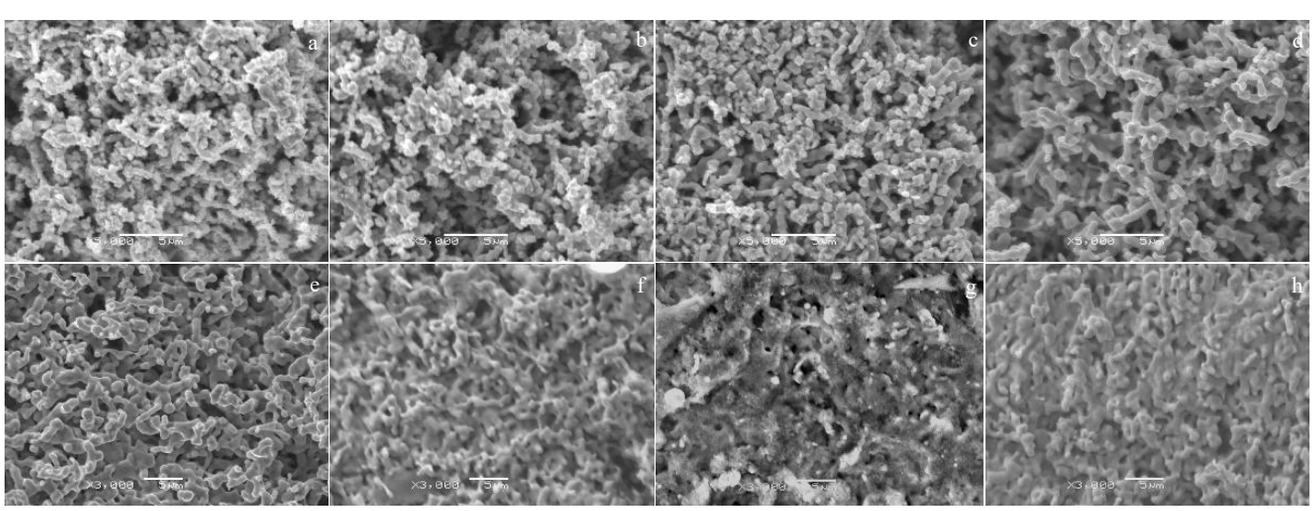

Fig.5 SEM morphologies of microporous nickel after sintering at different temperatures: (a) 300 °C, (b) 350 °C, (c) 400 °C, (d) 450 °C, (e) 500 °C, (f) 550 °C, (g) 600 °C, and (h) 650 °C

the melting point of pure nickel is 1453 °C. Thus, the further diffusion and flow occur at 750–1200 °C, and the pores are gradually spherized followed by shrinkage and densification. In this research, the particle size is 1 μm, indicating the fine powder; the specific surface area of powder particles is large, resulting in the increased grain boundary. These phenomena all improve the sintering activity, so the specimen becomes dense at about 650 °C. Only the sintering temperatures of 300, 350, and 400 °C can lead to the expected porosity of greater than 50%, which are 59.1%, 57.5%, and 53.7%, respectively.

As shown in Fig.5a–5c, the pore size is 0.3–2.5 μm, and the chain overlapping appears. During the sintering at low temperatures of 300 and 350 °C, the sintered particles are only in the bonding stage and not fully diffused. Thus, the bonding between powder particles is weak, resulting in little shrinkage. With increasing the sintering temperature, the pores are gradually reduced or closed, which is quite obvious at sintering temperatures of above 550 °C. The whole surface areas are flattened, as shown in Fig. 5e–5g. After sintering at 650 °C, the specimen becomes dense, and only the chain overlapping of original particles appears with a small number of closed pores. As shown in Fig.5h, the porosity is only 5.2%.

When the sintering temperature is 400 °C, the porosity of the specimen is 53.7%, which is still at a high porosity level. After sintering at 400 °C, a connected network structure with chain overlapping appears. The sintering neck is well developed. The pore size is 0.6–1.2 μm.

Fig. 6 shows the pore size distributions measured by mercury intrusion method of microporous nickel sintered at 400 °C. It can be seen from Fig. 6a that in the early stage of mercury intrusion, the large pores with diameter>500 nm exist. With increasing the pressure, the mercury inflow is maintained at about 0.148 mL/g. Meanwhile, the mercury enters the micropores with diameter<500 nm, and the total mercury intake of the specimen is 0.148 mL/g.

It can be seen from Fig. 6b that the maximum pore size is about 432.3 nm. The average pore diameter of microporous nickel specimen is 612.25 nm. The median pore size is about 652.08 nm. According to the particle size distribution curve, the pores with diameter of 500–700 nm account for 81.6%. The total specific surface area S of microporous nickel specimen can be calculated by Eq.(1), as follows:

$$S = \frac{1}{\gamma \cos\theta} \int_0^{v_{max}} P \mathrm{d}v \quad (1)$$

where γ is surface tension of 0.48 J/m^2; θ is wetting angle of 140°; v_{max} is the maximum mercury injection volume; v is mercury injection volume; P is pressure.

As a result, the porosity measured by the mercury intrusion method of microporous nickel sintered at 400 °C is 56.2%, the average pore size is 612.25 nm, and the total specific surface area is 0.969 m^2/g. In practical applications, the smaller the pores, the greater the capillary force, the larger the specific surface area, and the more the active sites. Thus, the high porosity is conducive to the multiphase flow conduction.

2.3 Mechanical properties

The microporous nickel is often assembled with dense metal through transition fit, which is subjected to compressive load in the manufacture process. Therefore, the compressive performance of microporous nickel under the actual load was characterized. The compressive stress-compressive strain curves of specimens sintered at different temperatures are shown in Fig.7, and the compressive speed is 1 mm/min.

Fig. 7a shows that the low strengths of 127 and 237 MPa at sintering temperatures of 300 and 350 °C are caused by the weak bonding between the particles, respectively. The crack propagates along the pores and breaks during compression. When the sintering temperature is higher than 400 °C, no obvious fracture can be observed and only the compressive deformation occurs, indicating that with increasing the temperature, the metallurgical bonding forms in specimen, the sintering neck is well developed, and the strength is further improved. No obvious fracture or yield phenomenon can be found with further increasing the temperature. The yield strength, namely specified plastic compressive strength $R_{pc0.2}$, of microporous nickel specimens sintered at different temperatures is shown in Fig. 7b. With increasing the sintering temperature, the yield strength of microporous nickel specimens is increased, and it is greater than 82 MPa when the sintering temperature is above 400 °C. When the sintering temperature increases to 550 °C, the strength fluctuates. At this sintering temperature, although the porosity is low, it still influences the strength as a defect. With further increasing the

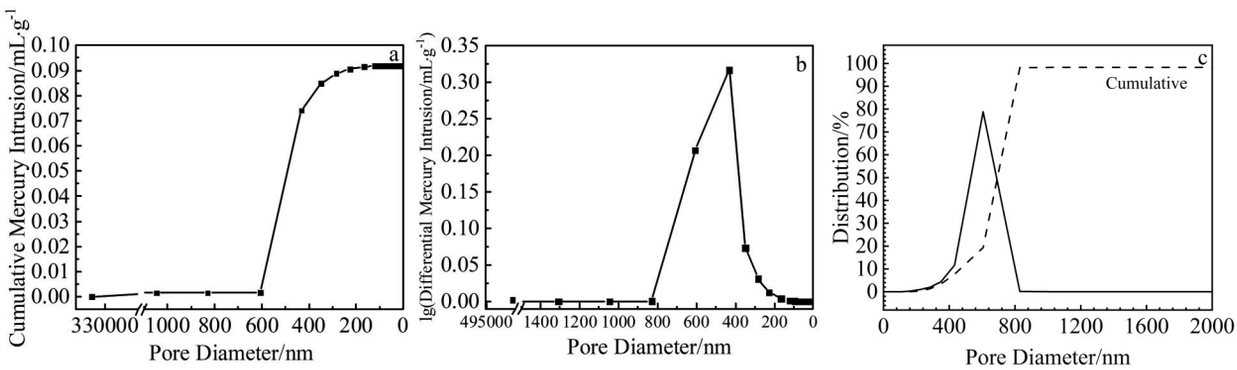

Fig.6 Pore size distributions of microporous nickel sintered at 400 °C: (a) relationship between cumulative mercury intrusion and pore size; (b) relationship between differential mercury intrusion and pore size; (c) pore size distribution

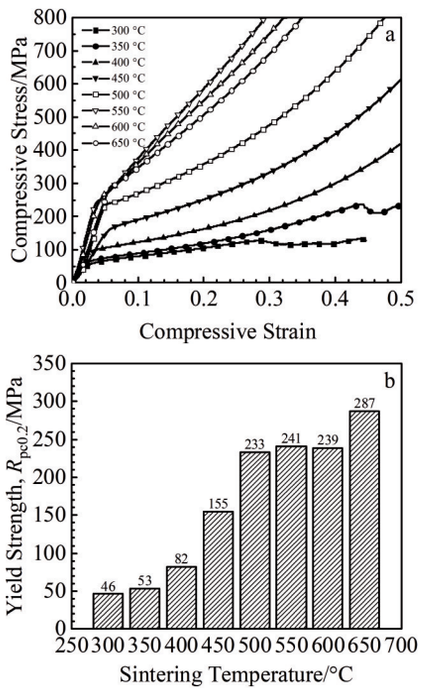

Fig.7 Compressive stress-compressive strain curves (a) and yield strengths (b) of microporous nickel specimens sintered at different temperatures

sintering temperature to 650 °C, the lowest porosity of 5.2% is obtained, the specimen becomes dense, and the highest strength of 287 MPa is achieved.

No obvious fracture occurs at the sintering temperatures of above 400 °C, and the compressive stress continues to rise after reaching a certain value. Even with high porosity, the microporous nickel retains the plastic toughness of the original metal nickel. The microporous connection structure forms a compressed carrier, exerting the pore buffer effect. The specimens sintered at low temperatures of 300 and 350 °C are fractured during compression. During these sintering process, only the weak bonding occurs between particles. The specimen strength is low, and the fracture occurs under small load. When the sintering temperature is higher than 400 °C, the sintering neck of the specimen is staggered to form a pore structure and a metallurgical combination, which causes good compressive strength and plasticity.

2.4 Effect of processing on pore structure

Microporous nickel used in special fields should have good machining performance for assembly accuracy, especially for heat transfer elements. The flow channel in porous elements can facilitate the multiphase flow exchange in the system and play the role of energy transmission. The difficulty of porous material machining is that the chip machining will deform and block the original pores, thus losing material function. Therefore, the porous materials are generally formed into the near-net shape. In this research, the modified processing improves the machinability of microporous nickel components, improves the assembly accuracy, and enhances the material function[25]. The machining performance of microporous nickel with high porosity was discussed through the strategy of sintered closed-hole followed by reopening process. The specimens sintered at 400 °C with high porosity and appropriate pore size were selected for analysis. In this experiment, the inner side of microporous nickel was prepared into channels, and the outer surface was machined to improve the accuracy. The dimensional accuracy of traditional porous materials is ±(0.5%–1%) of the machining size, while that after closed-hole machining is close to the accuracy level of dense materials, suggesting a great improvement in the machining accuracy of metal porous materials.

Fig. 8 shows the appearances and SEM morphologies of microporous nickel after hole opening treatment. Fig.8a shows the machined cylindrical surface. It can be seen that compared with the raw specimen, the surface area of the machined specimen is flatter and the pores are evenly distributed. This is due to the extrusion of the specimen along the feed direction during the chip cutting process, and the surface of nickel matrix tends to be flat. The closed pore part still maintains the sintered pore morphology due to the additives, and the pore size is less than 2 μm, as shown in Fig. 8b. According to Fig. 8c, the pores are smaller than those in the outer circular surface. Compared with those in the inner circular surface, the number of macropores in the outer circular surface is reduced, which is caused by the change in machining methods, and the pores are evenly distributed and dispersed. The local morphologies of microporous nickel are analyzed by the industrial computerized tomography (CT), as shown in Fig. 9. The selected area consists of large pores with size of 10–50 μm, which only account for 0.09‰ of the overall structure.

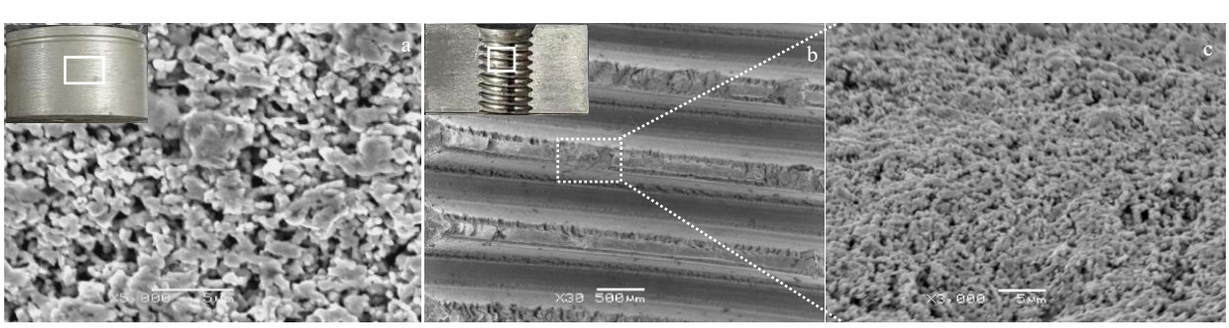

Fig.8 Appearances and SEM morphologies of processed specimens: (a) outer surface and (b, c) inner pores

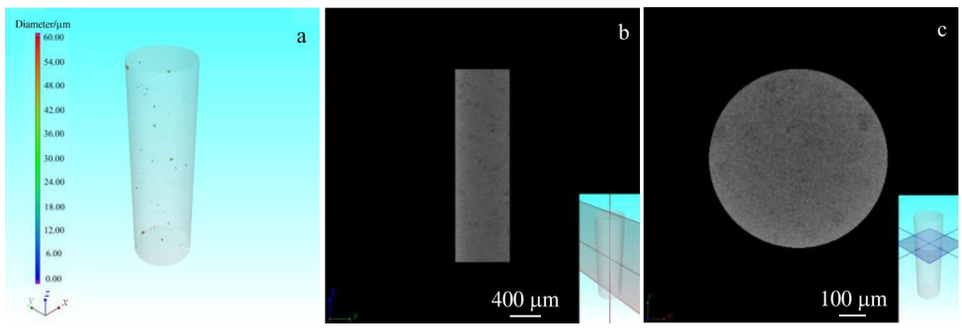

Fig.9 Selected area (a), axial section (b), and cross section (c) of CT scanning morphologies of microporous nickel after reopening treatment

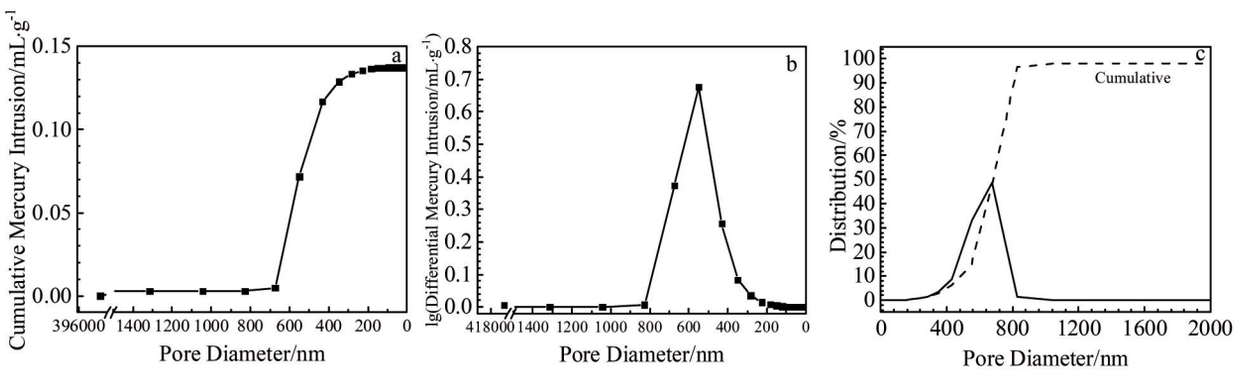

Fig.10 Pore size distributions of microporous nickel after hole opening treatment: (a) relationship between cumulative mercury intrusion and pore size; (b) relationship between differential mercury intrusion and pore size; (c) pore size distribution

The pores with other sizes account for a small number and cannot be effectively identified, indicating that the micropores are evenly distributed in the whole microporous nickel specimen. The overall pore size is small of less than 1 μm, inferring that the pores are at micron-level.

The pore size analysis by mercury injection method was conducted on the sintered microporous nickel after hole opening treatment, as shown in Fig. 10. It can be seen from Fig. 10a that the amount of mercury intrusion gradually increases and the mercury fills the whole pore. The pore size in the early stage is greater than 500 nm. With the gradual filling of small pores, the final amount of mercury intrusion is at 0.136 mL/g. According to Fig. 10b, the maximum pore size is 550.5 nm. Fig. 10c shows that the pore diameter is mainly located at around 600 nm, and the porosity is 78.9%, indicating the high porosity level. The average pore diameter after reopening treatment is 511.37 nm, which is slightly lower than that before reopening treatment (621.25 nm). The porosity is also reduced from 56.2% to 54.0% after reopening treatment. The pore diameter and porosity are reduced slightly due to the deformation of some pores caused by the extrusion of shear force in the reopening process. Under the action of pore filler, the original structure can be better maintained, whereas some parts are extruded, resulting in the slight decrease in the average pore diameter. The comparison of pore size before and after machining is shown in Table 3. After reopening treatment, the porosity and pore size of microporous nickel maintain the high level, which can meet the requirements of service performance and assembly accuracy. The specific surface area increases to 1.074 m^2/g.

Table 3 Comparison of pore size of microporous nickel before and after reopening treatment

Property	Before	After
Average pore diameter/nm	612.25	511.37
Median pore diameter/nm	652.1	557.1
Bulk density/$g\cdot cm^{-3}$	3.79	3.93
Apparent density/$g\cdot cm^{-3}$	8.67	8.55
Porosity/%	56.2	54.0
Specific surface/$m^2\cdot g^{-1}$	0.969	1.074

3 Conclusions

1) With increasing the sintering temperature from 300 °C to 650 °C, the porosity of microporous nickel is decreased from 59.1% to 5.2%, and its strength is gradually increased. When the sintering temperature is higher than 400 °C, the yield strength is greater than 82 MPa. When the sintering temperature is 650 °C, the yield strength reaches 287 MPa, and this compressive strength is the highest.

2) After sintering at 400 °C, the porosity measured by mercury injection method is 53.7% and the average pore diameter is 612.25 nm, which can meet the application requirements of high porosity and small pores.

3) After reopening treatment, the pore structure of microporous nickel maintains the original structure, and the

porosity maintains the high level. The porosity of microporous nickel sintered at 400 °C after reopening treatment is 54.0%, and the average pore diameter is 511.37 nm, which can also meet the requirements for assembly accuracy.

References

1 Ezugwu E O, Wang Z M, Machado A R. *Journal of Materials Processing Technology*[J], 1998, 86(1–3): 1

2 Ulutan D, Ozel T. *International Journal of Machine Tools & Manufacture*[J], 2011, 51(3): 250

3 Yang Ruicheng, Nie Furong, Zheng Liping *et al. Journal of Gansu University of Technology*[J], 2002, 28(4): 29 (in Chinese)

4 Li Meng. *Rare Metal Materials and Engineering*[J], 2010, 39(10): 1858 (in Chinese)

5 Zhang Yi, Wang Senlin, Li Caicai. *Rare Metal Materials and Engineering*[J], 2012, 41(3): 457 (in Chinese)

6 Hou Z Y, Yokota O, Tanaka T *et al. Catalysis Letters*[J], 2003, 89(1–2): 121

7 Lee Y J, Lee Y S, Cha J Y *et al. International Journal of Hydrogen Energy*[J], 2020, 45(38): 19 181

8 Li Y K, Zhang Q F, Chai R J *et al. ChemCatChem*[J], 2015, 7(9): 1427

9 Wang Qiangbing, Tang Huiping, Yang Baojun. *Materials China*[J], 2016, 35(2): 31 (in Chinese)

10 Wang Tianyao, Zhou Yun, Sun Yadong *et al. Chinese Journal of Rare Metals*[J], 2018, 42(12): 8 (in Chinese)

11 Bhattacharya A, Calmidi V V, Mahajan R L. *International Journal of Heat & Mass Transfer*[J], 2002, 45(5): 1017

12 Zhi Hao, Xi Zhengping, Tang Huiping *et al. Rare Metal Materials and Engineering*[J], 2009, 38(S3): 245 (in Chinese)

13 Ye Xinli, Zhang Junxiong, Xiang Junfeng *et al. Acta Materiae Compositae Sinica*[J], 2022, 39(8): 3794 (in Chinese)

14 Wang D D, Wang J X, Liu P J *et al. International Journal of Thermal Sciences*[J], 2020, 155: 106 445

15 Li Q F, Lan Z, Chun J *et al. International Communications in Heat and Mass Transfer*[J], 2021, 121: 105 123

16 Wang Dezhi, Wang Xiaoying, Zhou Pan *et al. Materials Science and Engineering of Powder Metallurgy*[J], 2014, 19(5): 687 (in Chinese)

17 Li Qiang, Gan Xueping, Li Zhiyou *et al. Materials Science and Engineering of Powder Metallurgy*[J], 2018, 23(4): 361 (in Chinese)

18 Li H, Liu R T, Chen J *et al. Journal of Materials Research and Technology*[J], 2020, 9(3): 3149

19 Yakomaskin A A, Afanasiev V N, Zubkov N N *et al. Journal of Heat Transfer*[J], 2013, 135(10): 101 006

20 Maydanik Y F. *Applied Thermal Engineering*[J], 2005, 25(5–6): 635

21 Putra N, Saputra A N, Bimo M I *et al. AIP Conference Proceedings*[J], 2012, 1440(1): 612

22 Zhang X F, Li X Y, Wang S F. *International Journal of Thermal Sciences*[J], 2012, 54: 188

23 Singh R, Nguyen T, Mochizuki M. *Applied Thermal Engineering*[J], 2014, 63(1): 406

24 Li H, Liu Z C, Chen B B *et al. Experimental Thermal and Fluid Science*[J], 2012, 37: 91

25 Wang Hao, Yang Kun, Huang Yuanping *et al*. *China Patent*, ZL113000841B[P], 2021 (in Chinese)

高孔隙率微孔镍的制备及性能

王 昊[1]，杨 坤[1]，王建忠[1]，石 英[1]，冯培忠[2]，黄愿平[1]，荆 鹏[1]，Farid Akhtar[3]

(1. 西北有色金属研究院 金属多孔材料国家重点实验室，陕西 西安 710016)

(2. 中国矿业大学 材料与物理学院，江苏 徐州 221116)

(3. 吕勒奥理工大学 材料科学部，瑞典 吕勒奥 97187)

摘 要：提出了一种烧结后闭孔加工再开孔的策略，通过粉末冶金方法和后续加工处理制备出了高孔隙率的微孔镍材料。采用粒径为1 μm的羰基镍粉为原料，研究了烧结工艺参数对多孔镍的孔隙性能和力学性能的影响。结果表明，在400 ℃烧结温度下，压汞法测得微孔镍的孔隙率为53.7%，平均孔径为612.25 nm。经加工处理后的压汞孔隙率为54.0%，平均孔径为511.37 nm，加工后孔隙结构仍符合应用要求，为多孔镍及其他多孔金属材料的制备开辟了一条新的途径。

关键词：高孔隙率；微孔结构；多孔镍；制备工艺；加工性能

作者简介：王 昊，男，1991年生，硕士，工程师，西北有色金属研究院金属多孔材料国家重点实验室，陕西 西安 710016，电话：029-86231095，E-mail：kirahi@126.com